Biophysical Chemistry 20 (1984) 1–21
Elsevier

BPC 00860

DYNAMIC LIGHT SCATTERING STUDY OF MUSCLE F-ACTIN *

Satoru FUJIME [a], Shin'ichi ISHIWATA [b] and Tadakazu MAEDA [a]

[a] *Mitsubishi-Kasei Institute of Life Sciences, Machida, Tokyo 194, and* [b] *Department of Physics, Waseda University, Shinjuku, Tokyo 160, Japan*

Received 21st January 1984
Accepted 27th February 1984

Key words: Dynamic light scattering; Fast Fourier method; Semidilute solution; F-Actin; Filament flexibility

By use of digital autocorrelation and fast Fourier methods, dynamic light-scattering studies of in vitro reconstituted muscle F-actin were made over a wide range of concentrations, 0.01–2 mg/ml F-actin. Measurements of correlation function $[g^1(t)]^2$ showed that a transition from a dilute to a semidilute regime for the Brownian motions of filaments occurred at around 0.3 mg/ml F-actin. Beyond this concentration, profiles of successively measured $[g^1(t)]^2$ showed very poor reproducibility. This resulted from the existence of very slow components, which could not be measured with a high statistical accuracy even for a measuring time of 3600 s/run. On the other hand, subtraction of these components automatically by an electronic circuit, $[\bar{g}^1(t)]^2$, or by computer processing, $[g_*^1(t)]^2$, resulted in a fairly good reproducibility of the profiles. The decay characteristics of $[g_*^1(t)]^2$ (and $[\bar{g}^1(t)]^2$) were very similar to those of $[g^1(t)]^2$ for dilute solutions. A theoretical model will be discussed which could account for the above situation. The time sequence $\{n(t,T)\}$ of photoelectron counts at a sampling time T of light scattered from semidilute solutions of F-actin was stored on magnetic tapes, and both power spectra $\bar{S}(f)$ and correlation functions $[\bar{g}^1(t)]^2$ were computed by taking the ensemble average over many short records with duration $1024T$. Since both $\bar{S}(f)$ and $[\bar{g}^1(t)]^2$ lacked frequency components lower than $1/(2048T)$ Hz, their profiles were highly reproducible. An analysis of $\bar{S}(f)$ confirmed our earlier results which had shown an apparent contradiction to later results by a correlation method. A comparison of $\bar{S}(f)$ and $[\bar{g}^1(t)]^2$ based on the same $\{n(t,T)\}$ clarified the reasons why the bandwidth Γ of $\bar{S}(f)$ largely differed from the bandwidth $\bar{\Gamma}$ of $[g^1(t)]^2$ and $[\bar{g}^1(t)]^2$. The temperature dependence of Γ suggested that F-actin would be flexible and that the flexibility parameter would change with temperature.

1. Introduction

Firstly, a brief introduction of the structural basis of muscle proteins is given. G-Actin is globular in shape. Its molecular mass is about 42 kDa. G-Actin polymerizes into F-actin (fibrous form) under physiological salt conditions. Based on observation by electron microscopy, a 'pearl-and-necklace' model is proposed for the ultrastructure of F-actin. F-Actin is a two-stranded helical polymer. The half-pitch of the helix is 36 nm and within this length, there are 13 G-actins. The total length (L) of F-actin varies according to polymerization conditions and, roughly speaking, is longer than 1 μm. As might be supposed from its structure, F-actin is slightly flexible. Tropomyosin is a rod-like protein. Its diameter is 2 nm and length 40 nm. When tropomyosin molecules are added to the solution of F-actin, they bind to F-actin and settle in the grooves of the F-actin helix and form tropomyosin strands. Myosin has two heads called subfragment-1 (S1) and binds to F-actin in the absence of ATP. Partial digestion by some kind of proteases produces heavy meromyosin (HMM) and S1.

Next, a brief review of F-actin studies by dynamic light scattering is given. Using an a.c.-coupled spectrum analyzer, the power spectra of light scattered from solutions of F-actin were first obtained by Fujime [1] and were analyzed by use of a

* A part of this study was presented at the NATO ASI on Application of Laser Light Scattering to the Study of Biological Motion, Maratea, Italy, June, 1982.

single Lorentzian having a half-width Γ. The Γ vs. K^2 relationship thus obtained has the form $\Gamma = AK^2 + B$ for $K^2 \geq 2 \times 10^{10}$ cm^{-2}, where A and B are constants and K the length of the scattering vector. However, it was very difficult to give reasonable meanings to the constants A and B. Based on a model of polymer dynamics, Fujime derived the following form for the homodyne power spectral density of scattered light [1]

$$S(K,f) = \sum_{\text{even } N \text{ and } M} \sum P_M(K) P_N(K) \times \frac{2DK^2 + (M+N)/\tau_1}{(2\pi f)^2 + \left[2DK^2 + (M+N)/\tau_1\right]^2} \quad (1)$$

where τ_1 is the relaxation time of the lowest bending mode of motion of the filament (and is equal to τ_2 given in our later publications [2,3]) and D the translational diffusion constant. The reasons why contributions from the rotational motion of the filament were ignored, were (i) $1/(6\theta) \simeq 1$ s for a filament with length $l \simeq 2$ μm is too long compared with such times as $1/(DK^2) \leq 10$ ms and $\tau_1 \leq 10$ ms, and (ii) the interfilament distance ($\simeq 300$ nm) in the solution at a few mg/ml F-actin is far shorter than the length of filaments (i.e., the rotational motion will be strongly restricted), whereas the amplitude ($\simeq 100$ nm) of the bending motion is comparable to or smaller than the interfilament distance (i.e., the bending motion will be almost free). Further simplifications were made: (a) the $M = N = 0$ term is too narrow to be correctly detected because of the lower frequency of the response function of the spectrum analyzer we used ($\simeq 20$ Hz); (b) the terms specified by large M and/or N weakly contribute to the far wing of the spectrum; and (c) because of the broad size distribution of in vitro reconstituted filaments, only an average spectrum will be detected. And finally the following form was assumed:

$$S(K,f) = \frac{2DK^2 + 1/\hat{\tau}}{(2\pi f)^2 + (2DK^2 + 1/\hat{\tau})^2} \quad (2)$$

where $1/\hat{\tau}$ is the $P_M P_N$-weighted average of $(M+N)/\tau_1$. Namely, Fujime assumed that A is related to the translational diffusion constant of, and B to the relaxation time of the bending motion of, the filament. Without a detailed computation of $P_M(K)$ the above formula is said to have no sound physical basis. However, the extensive results of Ishiwata and Fujime [4,5] under the assumption of eq. 2 showed that both A and B were delicately dependent on solvent conditions and the state of F-actin interacting with other muscle proteins such as tropomyosin, troponin and HMM, and also showed very good correlation with results by various techniques other than light scattering.

By using a digital correlator, the correlation functions of light scattered from solutions of F-actin and its complexes with HMM or S1 were studied by Carlson and co-workers [6,7]. The correlation functions for F-actin are highly nonexponential and the initial decay rate deduced from a cumulant expansion method has the form $\bar{\Gamma} = A(K^2)K^2$, where $A(K^2)$ is an increasing function of K^2. Later, Maeda and Fujime [8] reconfirmed this result, and further reported the observation of a very long tail (which decays in the range of tens of seconds) in the correlation functions.

Since the long-tail behavior of correlation functions is expected to arise from entanglements of long filaments such as F-actin in semidilute solutions, Oplatka and co-workers [9] studied F-actin and its complexes with HMM at relatively low actin concentrations. In order to avoid complexities resulting from sample polydispersity of in vitro reconstituted F-actin, Newman and Carlson [10] used intact thin filaments of scallop adductor muscle (F-actin-tropomyosin complex). Based on a theoretical model [1,2], Maeda and Fujime [3] succeeded in deducing the flexibility of the thin filament from the experimental result of Newman and Carlson.

During 1975–1980, the flexibility of F-actin complexed with other muscle proteins and in vivo thin filaments was extensively studied by various techniques other than light scattering [11–17]. All those studies supported our previous conclusions based on eq. 2. Thus, we have to overcome a difficult problem on the apparent discrepancy between $\Gamma = AK^2 + B$ and $\bar{\Gamma} = A(K^2)K^2$.

In this study, we will present mainly the experimental results on in vitro reconstituted F-actin and its complexes with other muscle proteins in a

relatively wide range of actin concentrations, studied by digital autocorrelation and fast Fourier methods. Then, we will discuss the experimental results based on our recent theoretical model given elsewhere [18].

2. Methods

2.1. Correlation functions and power spectra

Firstly, the basic idea of our technique is introduced. We follow the method of Rice [19]. Let us consider a model situation where a stochastic signal $i(t)$ is recorded for a long time. Let us construct an ensemble by cutting the record of $i(t)$ up into strips (subsets) of equal length $\mathscr{T}$:

$$\{i_k(t)\} \quad k=1, 2, \ldots \quad \text{and} \quad (k-1)\mathscr{T} \le t \le k\mathscr{T} \tag{3}$$

We develop $i_k(t)$ in a Fourier series

$$i_k(t) = \sum_{n=1} [a_n \cos(2\pi f_n t) + b_n \sin(2\pi f_n t)] \tag{4}$$

where $f_n = n/\mathscr{T}$. We assume $\langle i_k(t)\rangle_k = 0$, where the angular brackets denote time average within each record k. The Fourier coefficients are highly variable from one record to another. The power in the nth component is

$$P_n = [a_n \cos(2\pi f_n t) + b_n \sin(2\pi f_n t)]^2 \tag{5}$$

Thus, we have

$$\langle P_n\rangle_k = [\langle a_n^2\rangle_k + \langle b_n^2\rangle_k]/2 \tag{6}$$

Now, the ensemble average, denoted by a bar over the quantity, is an average over a large set of independent records k. For a random process, we have $\overline{a_n} = \overline{b_n} = \overline{a_n b_m} = 0$ and $\overline{a_n a_m} = \overline{b_n b_m} = \sigma_n^2 \delta_{nm}$. Thus, from eq. 6 the ensemble average of the time average power dissipation associated with the nth component of $i(t)$ is given by

$$\overline{\langle P_n\rangle_k} = \sum_k \langle P_n\rangle_k / \sum_k 1 = \sigma_n^2 \tag{7}$$

Let $P(f)$ be the power spectrum of $i(t)$. Then, we have

$$P(f_n)\Delta f_n = \sigma_n^2 \quad \text{with} \quad \Delta f_n = f_{n+1} - f_n = 1/\mathscr{T} \tag{8}$$

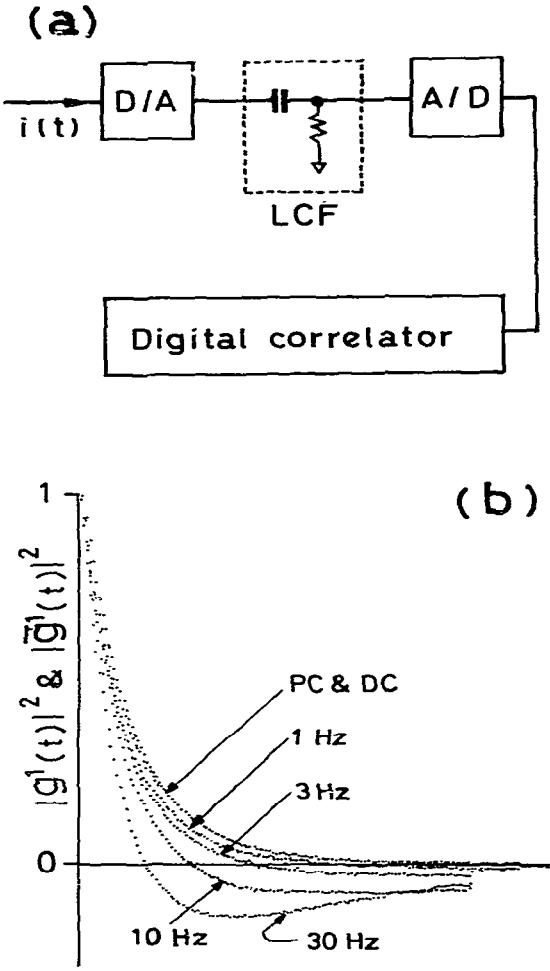

Fig. 1. Effect of a low-cut filter. (a) Schematic illustration of a circuit for low-cut filtering. D/A and A/D, digital-to-analog and analog-to-digital converters, respectively; and LCF, a low-cut filter. (b) Examples of correlation functions showing the effect of the low-cut filter. PC, photon-counting, i.e., the digital signal was directly fed to the correlator; DC, LCF was removed, and values given indicate the critical frequency ($\gamma/2\pi$ in Hz units) of the low-cut filter. Scattering sample was a dilute solution of polystyrene latex spheres.

The correlation function of $i(t)$ will be given by

$$G(\tau) = \overline{\langle i(t)i(t+\tau)\rangle}_k = \sum_n \sigma_n^2 \cos(2\pi f_n \tau) \quad (9)$$

From eqs. 8 and 9, we have

$$G(t) = \int_{-\infty}^{\infty} S(f) e^{2\pi i f t} \mathrm{d}f \quad (10)$$

where $S(f) = [P(f) + P(-f)]/2$.

Consider a situation where $i(t)$ is first fed to a low-cut filter (LCF) and then to a correlator (Fig. 1a). In this situation, the signal to the correlator lacks its low-frequency components, i.e., a_n and b_n for small n values in eq. 4. Thus, it is evident from the above consideration that

$$\bar{G}(t) = \int_{-\infty}^{\infty} [1 - F(f)]\, S(f) e^{2\pi i f t} \mathrm{d}f$$

$$= G(t) - \tilde{F}(t) * G(t) \quad (11a)$$

$$\bar{S}(f) = [1 - F(f)]\, S(f) \quad (11b)$$

where the asterisk denotes convolution and $\tilde{F}(t)$ is the Fourier transform of $F(f)$. (Here and hereafter, the bar over $G(t)$, $g(t)$ or $S(f)$ indicates that the low-frequency components of the signal have been filtered out.) The function $[1 - F(f)]$ is assumed, for convenience of algebraic manipulation, to be given by

$$F(f) = \frac{\gamma}{2} \frac{2\gamma}{(2\pi f)^2 + \gamma^2} \quad \text{or} \quad \tilde{F}(t) = \frac{\gamma}{2} e^{-\gamma t} \quad (12)$$

where $\gamma/2\pi$ is the critical frequency in hertz of the low-cut filter. The $[1 - F(f)]$ in this particular choice of $F(f)$ just corresponds to the frequency characteristics of a low-cut filter consisting of a two-stage cascade RC network. Then, we have for $G(t) = \exp(-\Gamma t)$, for example,

$$\tilde{F}(t) * G(t) = \gamma \frac{\Gamma e^{-\gamma t} - \gamma e^{-\Gamma t}}{\Gamma^2 - \gamma^2} \quad (13)$$

Experimental verification of the validity of eq. 11a with eq. 13 was made by measuring the intensity of light scattered from a dilute solution of polystyrene latex spheres (fig. 1b).

Let us consider another model situation, where $i(t)$, or $n(t)$ in a photon-counting experiment, is recorded with a sampling time T (in s). Then, we have a set of sampled values of $i(t)$ such as $i(t,T)$, $i(t+T,T),\ldots,$ $i(t+mT,T),\ldots,$ which we simply write as $\{i(m)\}$. We divide this big set into many subsets $\{i(m)\}_0$, $\{i(m)\}_1$, $\ldots$, $\{i(m)\}_k$, $\ldots$, where $\{i(m)\}_k$ is such a subset as it contains components $i(N_k)$, $i(N_k+1)$, $\ldots$, $i(N_k+N-1)$ and $N_k = kN$. (Note that $\mathscr{T} = NT$, cf. eq. 3.) Now, we have the correlation function $G_k(t)$ and the power spectrum $S_k(f)$ for each of the above subsets. According to Rice [19], the correlation function $G(t)$ and the power spectrum $S(f)$ for the big set are given by the ensemble average of $G_k(t)$ and $S_k(f)$ over all subsets k, respectively. Here we have to take account of the Nyquist sampling theorem. For a sampling time T, we do not have any information on frequency components higher than $1/2T$ (Hz). In addition to this, for data points N of each subset, say 1024, we do not have any information on frequency components lower than $1/2NT$ (Hz). When we compute $S_k(f)$ by use of a fast Fourier transform (FFT) algorithm, we subtract the mean value of $i(m)$ from each of sampled values, i.e., $\{i(m) - \langle i\rangle\}_k$. The mean value $\langle i\rangle = \langle i(m)\rangle_k$ for any subset k does not correspond to the d.c. component of $i(t)$ during the time interval for the subset k, but it contains frequency components lower than $1/2NT$(Hz). Fig. 2 depicts the frequency characteristics of an 'FFT spectrum analyzer.' Likewise, when we adopt the usual definition of the baseline level of a correlation function, the baseline level B_k of $G_k(t)$ is given by $N\langle i(m)\rangle_k^2$. The summation of B_k over all k is not equal to the baseline level B of $G(t)$. This arises from the fact that $\langle i(m)i(m+N)\rangle \neq \langle i(m)i(m+\infty)\rangle$ for a finite value of N, say 1024. The correlation function $G_k(t) - B_k$ has no frequency components higher than $1/2T$ and lower

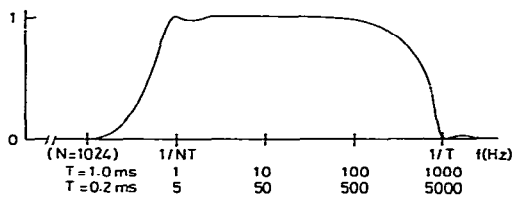

Fig. 2. Schematic illustration of the frequency response of an 'FFT spectrum analyzer'.

than $1/2NT$. Thus, we have

$$\bar{G}(t) = \text{ensemble average of } G_k(t) - B_k \quad (14a)$$

$$\bar{S}(f) = \text{ensemble average of } S_k(f) \quad (14b)$$

where the critical frequency of a low-cut filter is close to $1/2NT$ (Hz). The consideration given above is important in what follows.

2.2. Electronics

We used a 128-channel, single-clipped digital correlator, which had been made in our laboratory according to the design principle described by Chen et al. [20], and interfaced with a minicomputer mentioned below. Our correlator has 16 extra channels whose delay time starts from $128T(1+M)$, where T is the channel time (sampling time) and $M = 1$, 2 or 3. For the discussion that follows, we define the following four types of normalized correlation functions:

$$\beta[g^1(t)]^2 = \frac{1+\bar{n}}{1+k}[G^2(t) - G^2(\infty)]/G^2(\infty) \quad (15a)$$

$$[g^1(t)]^2 = [G^2(t) - G^2(\infty)]/[G^2(T) - G^2(\infty)] \quad (15b)$$

$$[g_-^1(t)]^2 = [G^2(t) - G^2(\overline{512T})]/[G^2(T) - G^2(\overline{512T})] \quad (15c)$$

$$[\bar{g}^1(t)]^2 = [\bar{G}^2(t) - \bar{G}^2(\infty)]/[\bar{G}^2(T) - \bar{G}^2(\infty)] \quad (15d)$$

where $G^2(t)$ denotes the time correlation function of the intensity of scattered light, $G^2(\infty) \equiv B$ the baseline level, $G^2(\overline{512T})$ the average of the above-mentioned 16 extra channels for $M = 3$ and $t = (1 + n)T$ with $n = 0, 1, \ldots, 127$, and $\bar{n}$ and k denote the mean counts per channel time and the clip level, respectively. Without extrapolation to $t = 0$, we do not know the value of $G^2(0)$, so that we used $G^2(T)$ instead of $G^2(0)$.

To record sampled values of $\{n(t + mT, T)\}$ and compute correlation functions $G_k(t)$ and power spectra $S_k(f)$ in eq. 14, we used the hardware system shown in fig. 3. 16 kilowords of memory were used for the data accumulation area. Every time this area was filled up, data on memory were transferred to a magnetic tape in units of 4 kilowords by a free format mode in a machine level. Our minicomputer (Nippon Data General, Model 02/30) installed hardware multiply/divide and

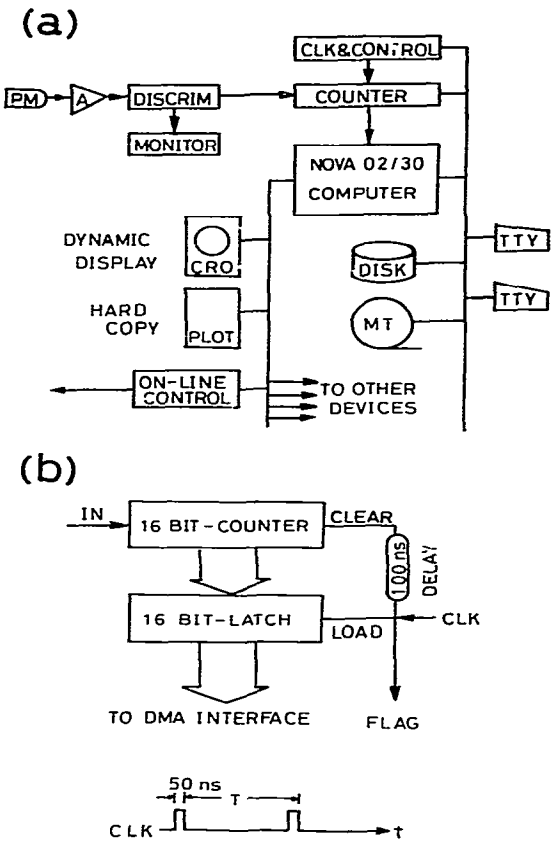

Fig. 3. Schematic illustration of the electronics system. (a) Computer-controlled hardware system. PM, photomultiplier tube; A, fast preamplifier; DISCRIM, amplifier/discriminator; CLK & CONTROL, a clock signal generator and a controller for COUNTER (see b); and NOVA 02/30, a minicomputer (Nippon Data General) equipped with hardware multiply/divide and floating point units. (b) A 16 bit-counter/latch circuit and a waveform of the clock signal, which enable registering of $n(t + mT, T)$ in a direct memory access (DMA) mode in a contiguous manner.

floating point units. The former was used for computation of $G_k(t)$ and the latter for computation of $S_k(f)$. For $N = 1024$, computation times were 3 s for $G_k(t)$ with 100 delay points and 1 s for $S_k(f)$. We also used an Eclipse minicomputer (Nippon Data General, Model S-140) for off-line computation. We sometimes placed the D/A-LC-A/D circuit in fig. 1 between DISCRIM and COUNTER in fig. 3. Using the same data on magnetic tapes, we computed both correlation functions and power spectra defined in eq. 14 for $N = 1024$.

2.3. Spectrometer

The spectrometer we used was a conventional one. A 488 nm beam from an argon ion laser (Lexel, Model 95) was focussed and passed through a sample cell made of pyrex glass tubing (outer diameter, 10 mm; wall thickness, 0.8 mm). The beam diameter at the scattering volume was about 0.1 mm. The sample cell was placed in a thermostatted oil bath mounted on an adaptor fixed to the center piece of a rotary table (300 mm diameter) for a milling machine. After passing through the sample cell the laser beam was adsorbed by a piece of a heavily colored glass plate in the oil bath in order to avoid back-reflection of the light from the glass/air boundary at the exit. To avoid moistening of the glass wall of the oil bath during measurements at low temperatures, the wall surface was constantly dried by nitrogen gas from a liquid-nitrogen container (with a small electric heater in it). On an arm tightly fixed to the rotary table, two pinholes, an interference filter and a photomultiplier housing (Ortec 9201) were mounted. The first pinhole (0.1–0.5 mm diameter in steps of 0.1 mm) was at about 150 mm from the sample cell and the second (0.5–0.1 mm diameter in steps of 0.1 mm) at 200 mm from the first pinhole. An RCA-8850 photomultiplier tube powered by an Ortec 456 high-voltage supply was used, and its output was fed to a fast preamplifier (Ortec 9301) and then to an amplifier/discriminator (Ortec 9302). The spectrometer and its accessories were mounted on a vibration-free table.

2.4. Materials

Muscle proteins were obtained from rabbit back and leg white muscle. Dry muscle was prepared by almost the same method as that of Straub [21], except that the regulatory proteins were removed before acetone treatment of myosin-extracted minced muscle. G-Actin was purified according to the method of Spudich and Watt [22] with slight modifications. Tropomyosin (TM) was prepared from native tropomyosin by using isoelectric precipitation and ammonium sulfate fractionation [23]. To prepare F-actin, G-actin filtered through a membrane filter (pore size 0.05 μm; Millipore Co.) was polymerized in the optical cell mentioned before at 0 °C under 0.1 M KCl, 1 mM $MgCl_2$, 10 mM Tris-HCl (pH 8.0) and 0.5 mM ATP. An F-actin-TM complex was prepared by polymerizing G-actin in the optical cell on adding a TM solution containing high salt which had been filtered through a membrane filter (pore size 0.22 μm). After polymerization, the actin concentration was decreased and adjusted to an appropriate value by adding the above solvent. Myosin subfragment-1 (S1) and heavy meromyosin (HMM) were prepared according to the method of Weeds and Pope [24] by chymotriptic digestion of myosin which had been purified as described by Szent-Györgyi [25] with slight modifications. An F-actin-S1 complex was obtained by adding S1 filtered through a membrane filter (pore size 0.22 μm) to the above F-actin solution before dilution. After ATP was hydrolyzed, the solution was diluted to 0.01 mg/ml F-actin by adding the above solvent without ATP. An F-actin-HMM complex was obtained by adding HMM (not filtered through a membrane filter) to the above F-actin solution before dilution. This mixing procedure was made in such a way to attain a final concentration of 0.5 mg/ml F-actin and a weight ratio of F-actin to HMM of 1:1–1:8. Both solvent and distilled water were filtered just before use (pore size 0.025 μm). The volume of filtrates was determined by their weight with an error of less than a few percent. The protein concentration was determined by a biuret method. ATP was purchased from Boehringer Mannheim Co., and other chemicals were of reagent grade.

3. Experimental

Fig. 4 shows 10 correlation functions successively measured for 300 s/run for a solution of 1 mg/ml F-actin. Fig. 4a and b shows examples of $\beta[g^1(t)]^2$ and $[g^1(t)]^2$, respectively. The profiles of correlation functions are largely different from run to run. However, this does not imply the time evolution of correlation functions associated with some change in scatterers in solution, because there was absolutely no definite trend in the appearance of profiles with time. Strong nonreproducibility of the profiles of correlation functions might result from the contribution of very slowly decaying components, because $[g^1_*(t)]^2$ in fig. 4c and $[\bar{g}^1(t)]^2$ (with $f_0 \equiv \gamma/2\pi = 0.1$ Hz) in fig. 4d

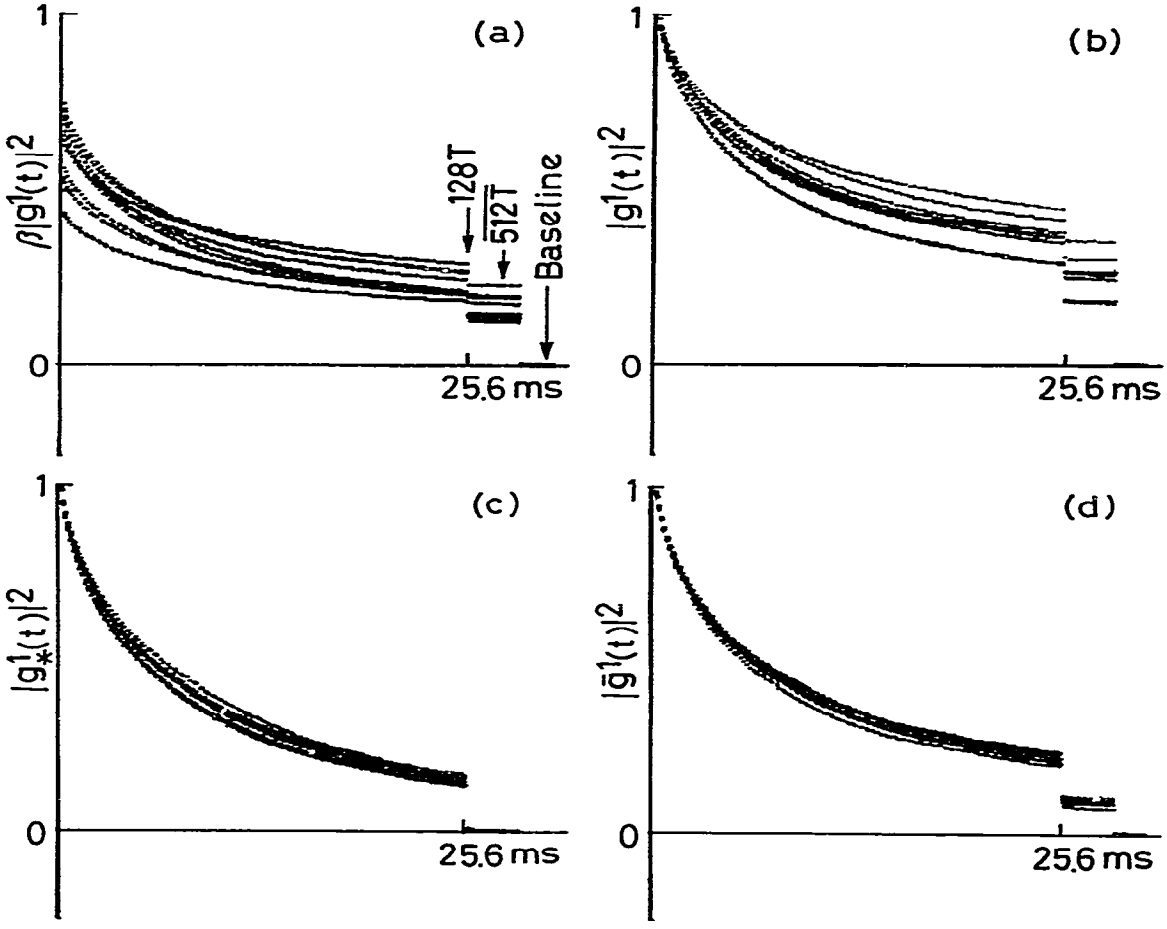

Fig. 4. Correlation functions (10 runs each) of the intensity of light scattered from a solution of F-actin at 1 mg/ml. Data accumulation period = 300 s/run, temperature = 5 °C, $T = 0.2$ ms and $K^2 = 0.9 \times 10^{10}$ cm^{-2} (scattering angle 32°). (a–c) Different plots of the same data, and $\gamma/2\pi = 0.1$ Hz in d.

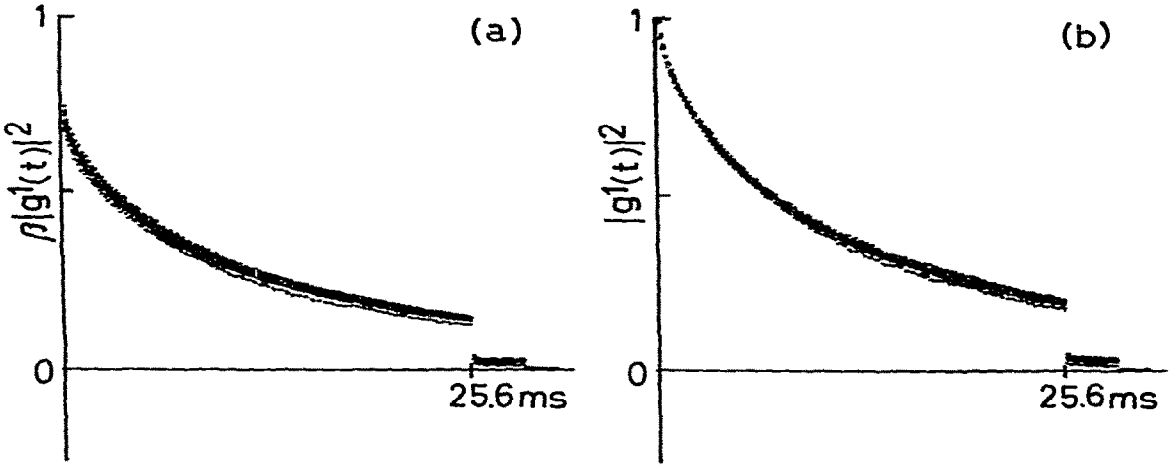

Fig. 5. Correlation functions (10 runs each) of the intensity of light scattered from a solution of F-actin at 0.2 mg/ml. Data accumulation period = 300 s/run, temperature = 5 °C, $T = 0.2$ ms and $K^2 = 0.9 \times 10^{10}$ cm^{-2}. (a and b) Different plots of the same data.

show better reproducibility. Fig. 5 shows 10 correlation functions successively measured for 300 s/run for a solution of 0.2 mg/ml F-actin. Here, the profiles of correlation functions, both $\beta[g^1(t)]^2$ and $[g^1(t)]^2$, have good reproducibility, and no long tail in correlation functions, inferred from the value of $[g^1(\overline{512T})]^2$, can be seen. Very large far-point values of correlation functions in fig. 4a and b may suggest the possibility that there was an occupation number fluctuation of large aggregates in the scattering volume at high concentrations of F-actin. At the moment, however, we do not believe this to be likely. We have several pieces of reasonable evidence to support this statement. First of all, correlation functions measured at different scattering volume, keeping the coherence condition unaltered, showed the same decay behavior. Single-clipped, scaled and full correlation functions showed the same decay behavior. The experimental excess amplitude, β in eq. 15a, had a value of 0.8 at the most. It did not exceed unity. (Its value for a dilute solution of polystyrene latex spheres was about 0.8 at the same machine condition.) Although more evidence may be required for our conclusion, we believe that strong nonreproducibility of the profiles of, and large far-point values of, correlation functions at high actin concentrations arise from very slow Gaussian fluctuations.

Fig. 6 shows examples of $[g^1(t)]^2$ at low actin concentrations. In the case of F-actin-S1 complexes, i.e., fig. 6c and d, a very large excess of S1 was added at low actin concentrations in order to decorate F-actin fully with S1. Due to this fact, free S1 molecules in the solution also contributed to the correlation functions. The very fast decay at short delay times in fig. 6c resulted from the contribution of free S1 molecules. (The fast component from free S1 would almost decay within the first 10 channels.) At low actin concentrations, both $\beta[g^1(t)]^2$ (not shown here) and $[g^1(t)]^2$ showed very good reproducibility in their profiles and very small far-point values. As a measure of the contribution from slowly decaying components, let us define

$$R = \left[g^1(\overline{512T})\right]^2 / \left[g^1(128T)\right]^2 \qquad (16)$$

Fig. 7 shows the R vs. concentrations of F-actin. The R values drastically changed at F-actin con-

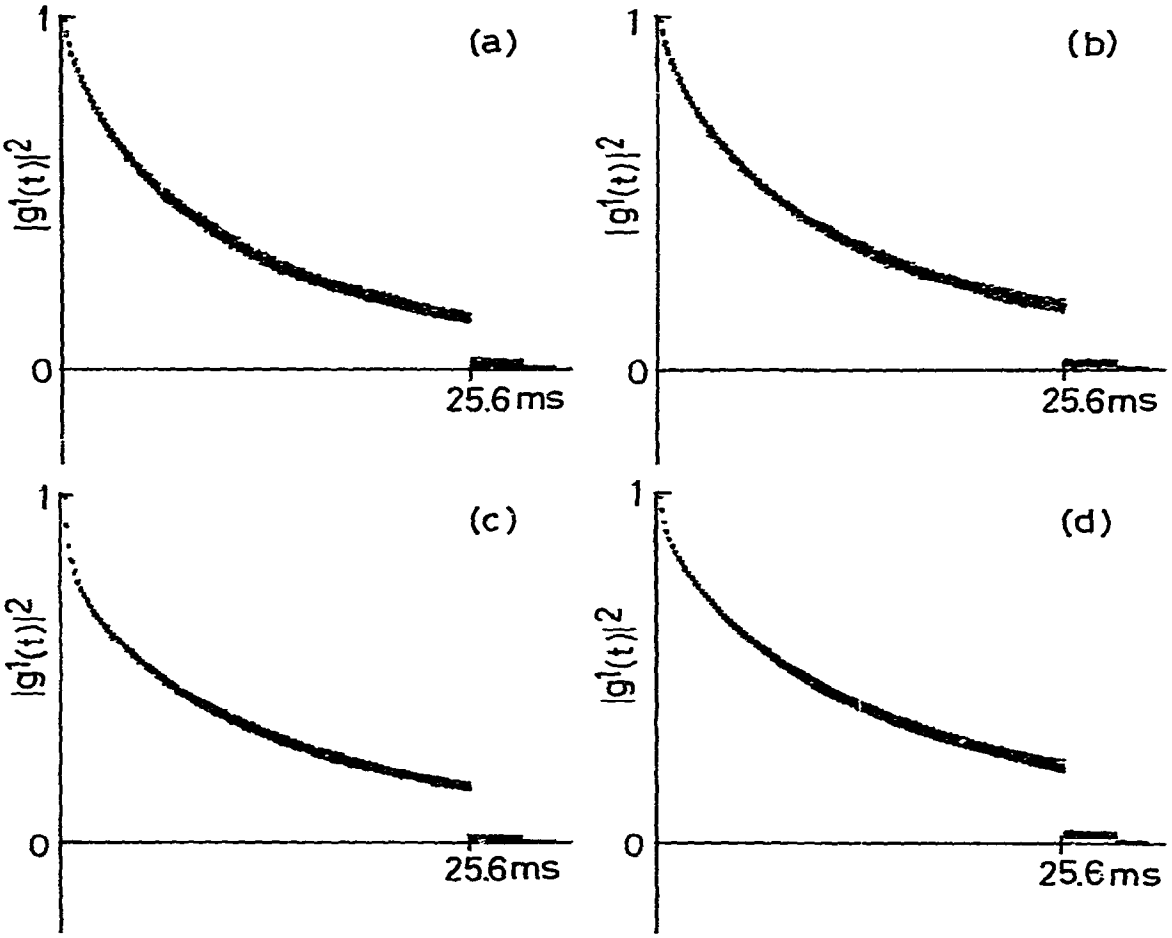

Fig. 6. Correlation functions (10 runs each) of the intensity of light scattered from solutions of F-actin and F-actin-S1 complexes at low actin concentrations. Data accumulation period = 300 s/run, temperature = 5 °C, $T = 0.2$ ms and $K^2 = 0.9 \times 10^{10}$ cm^{-2}. (a) 0.05 mg/ml F-actin, (b) 0.1 mg/ml F-actin, (c) 0.01 mg/ml F-actin and 1.25 mg/ml S1 and (d) 0.05 mg/ml F-actin and 1.25 mg/ml S1.

centrations in the range 0.2–0.5 mg/ml. However, the decay characteristics of $[g^1_*(t)]^2$ were rather similar, irrespective of the F-actin concentrations as shown by the values of $[g^1_*(128T)]^2$ in fig. 7.

Fig. 8 shows another example of correlation functions. A poor reproducibility of the profiles of correlation functions measured for 300 s/run (fig. 8a) was improved very little even when we measured them for 3600 s/run (fig. 8b). On the other hand, when we cut off the frequency components lower than 0.3 Hz, rather good reproducibility of the profiles of $[\bar{g}^1(t)]^2$ was observed even for a measuring time of 300 s/run (fig. 8c), and very good reproducibility was observed for a measuring

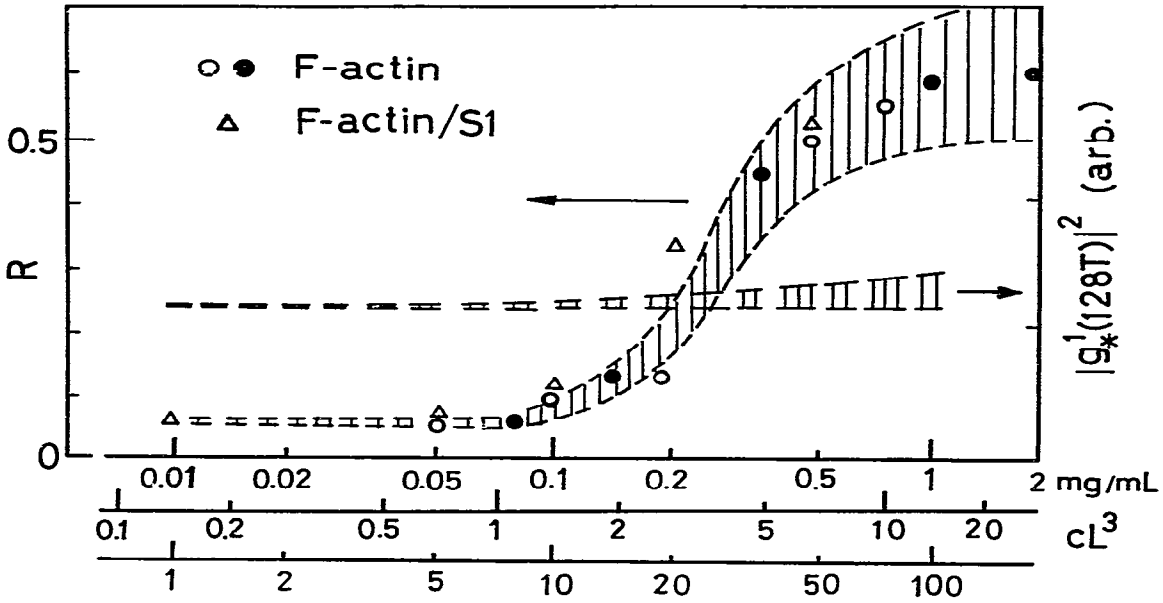

Fig. 7. R and $[g^1_*(128T)]^2$ vs. concentrations of F-actin (average of 30–90 runs per point). The abscissa is scaled also in cL^3 with $L = 0.7$ and 1.4 μm (see section 4). Experimental conditions were the same as those in figs. 4–6. $[g^1_*(128T)]^2$ values for F-actin/S1 were a little larger than those for pure F-actin for all concentrations studied.

time of 4500 s/run (fig. 8d). A measuring time of 3600 s is not long enough to observe such slowly decaying components with a high statistical accuracy.

Fig. 9 shows examples of correlation functions $[\bar{g}^1(t)]^2$ defined in eq. 14a. Even for a solution at 1 mg/ml F-actin, relatively good reproducibility of the profiles of correlation functions was observed for an effective measuring time of 80 s/run (i.e., the average of 400 $[G_k(t) - B_k]$ values). This is a natural consequence of the fact that the frequency components lower than 2.5 Hz ($T = 0.2$ ms and $N = 1024$) were filtered out by subtracting the mean counts, i.e., $\{n(t + mT, T) - \langle n \rangle\}_k$. The solid lines in fig. 9 represent the single exponentials whose decay rates were adjusted such that their initial parts fitted the experimental ones. Corresponding to a large deviation between the observed correlation functions and single exponentials, the power spectra defined in eq. 14b have large components in low-frequency regions (fig. 10). Note that the delay time of 10 ms in a correlation function corresponds to the frequency of $1/(10\ \text{ms} \times 2\pi) = 17$ Hz in a power spectrum. We have to take account of the fact that in our particular case, the initial decay rates of correlation functions have larger values, whereas the half-height widths of corresponding power spectra have smaller values.

As mentioned in section 1, our earlier results were obtained by using the a.c.-coupled spectrum analyzer. To compare the present results with the previous ones, the FFT spectra were modified by using the relationship in eq. 11b, where $\gamma/2\pi$ was chosen to be 30 Hz, the equivalent overall frequency characteristics of our previous spectrum analyzer. Fig. 11 shows some examples of the spectra thus obtained. We also recorded the sampled values of $\{n(t + mT, T)\}$, placing the D/A–LCF–A/D circuit in fig. 1 between DIS-

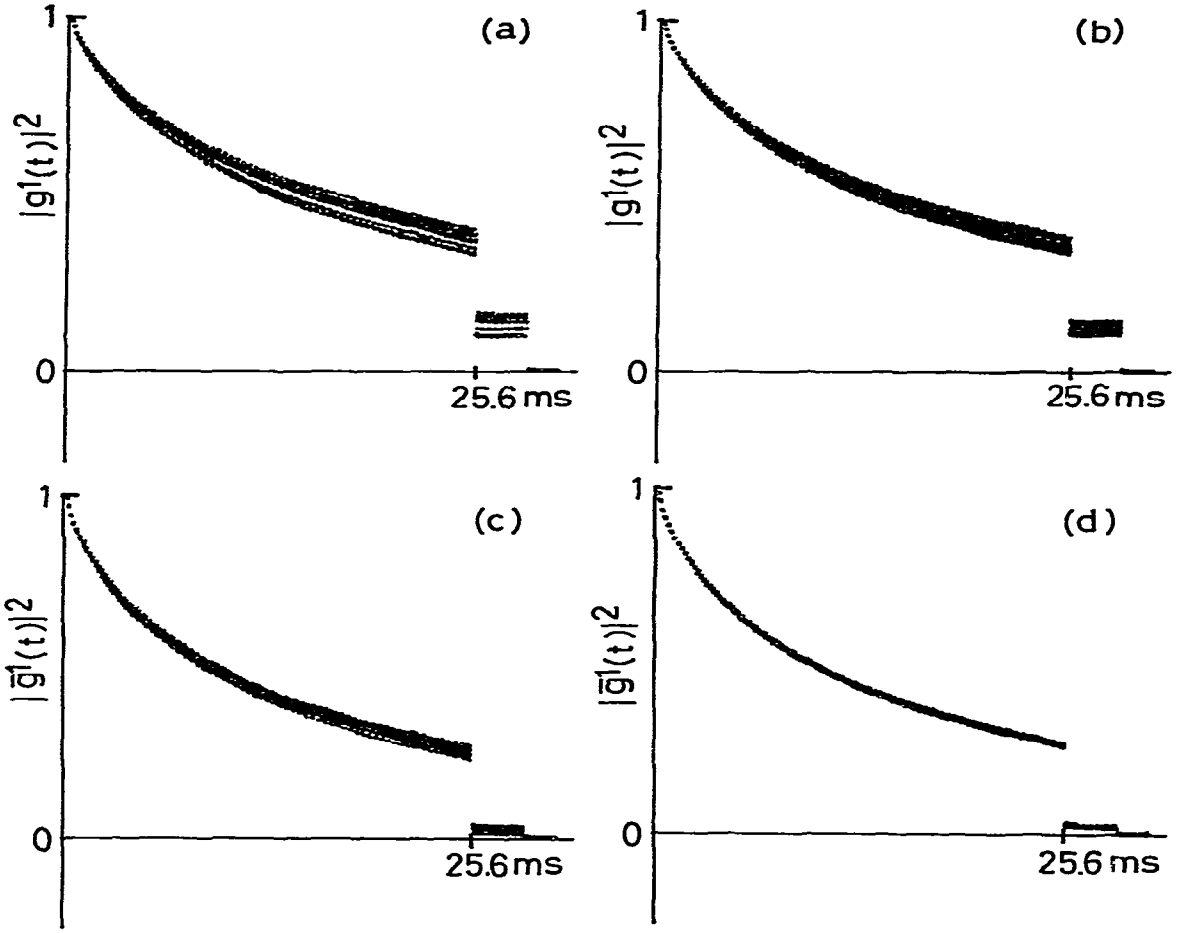

Fig. 8. Correlation functions (10 runs each) of the intensity of light scattered from a solution of F-actin/S1 at 0.2 mg/ml F-actin and 1.25 mg/ml S1. $[g^1(\tau)]^2$ at the measuring time of 300 s/run (a) and 3600 s/run (b). $[\bar{g}^1(\tau)]^2$ at the measuring time of 300 s/run (c) and 4500 s/run (d). (c and d) $\gamma/2\pi = 0.3$ Hz. Temperature = 5 °C, $T = 0.2$ ms and $K^2 = 0.9 \times 10^{10}$ cm^{-2}.

CRIM and COUNTER in fig. 3. By setting $\gamma/2\pi = 30$ Hz, we could obtain the FFT spectra very close to those in fig. 11 without any modification with $[1 - F(f)]$ in eq. 11b. The power spectra in the latter case just correspond to our earlier ones. The solid lines in fig. 11 represent the least-squares fitted curves to

$$\bar{S}(f) = P\frac{\Gamma}{f^2 + \Gamma^2} + Q \quad (P/\Gamma + Q = 1) \qquad (17)$$

where P and Q are constants independent of frequency. The Q contains contributions from

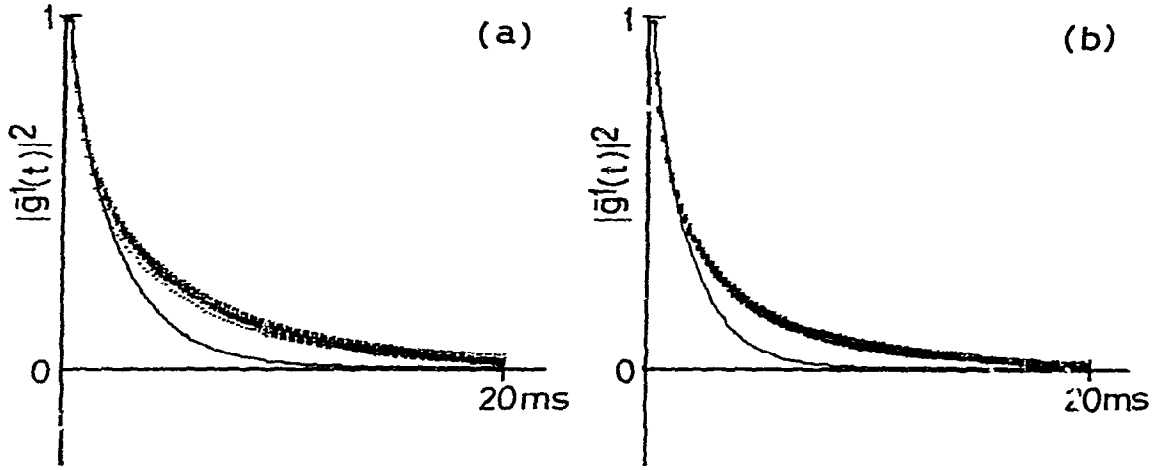

Fig. 9. Correlation functions (12 runs each) of the intensity of light scattered from a solution of F-actin at 1 mg/ml. $T = 0.2$ ms, $N = 1024$, temperature = 15 °C, effective measuring time = 80 s/run and the scattering angle = 30 ° (a) and 50 ° (b). (———) Single exponentials (see text).

high-frequency components as well as the frequency-independent shot noise. The magnitude of Q was less than 0.05 at scattering angles lower than 70 °, but became 0.1–0.15 at higher scattering angles. Because it is difficult to subtract the contribution to Q from the shot noise in the present FFT spectra, a quantitative discussion on K-dependent Q values is not possible.

Fig. 12a shows the Γ vs. K^2 relationship of the spectra $\bar{S}(f)$ modified with eq. 11b. This result is

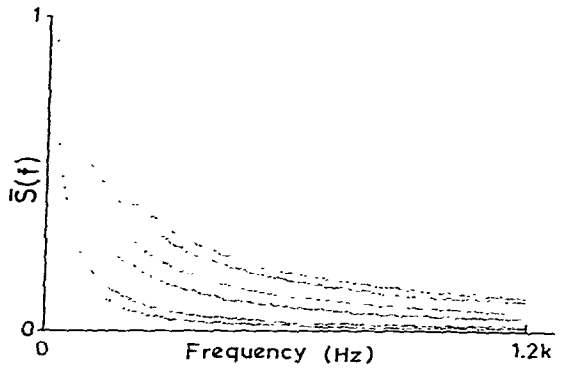

Fig. 10. Power spectra (average of 12 runs) of the intensity of light scattered from a solution of F-actin at 1 mg/ml. Data used for this computation were the same as those for correlation functions in fig. 9. Scattering angles: 30, 50, 70, 90, 110 and 130 °, respectively, from narrow to wide spectra.

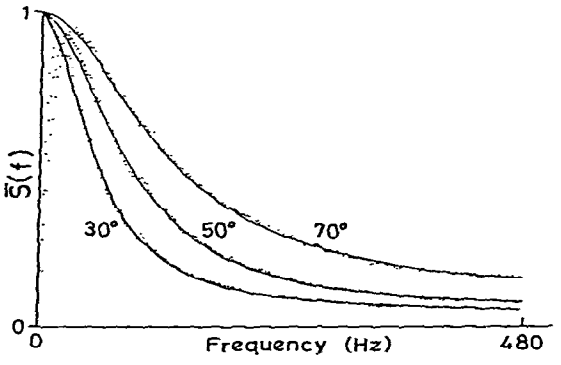

Fig. 11. Power spectra (average of 10 runs) of the intensity of light scattered from a solution of F-actin at 1 mg/ml. $T = 1$ ms, $N = 1024$, data accumulation period = 400 s/run and temperature = 15 °C. The FFT spectra were modified by use of eq. 11b with $\gamma/2\pi = 30$ Hz. For details, see text.

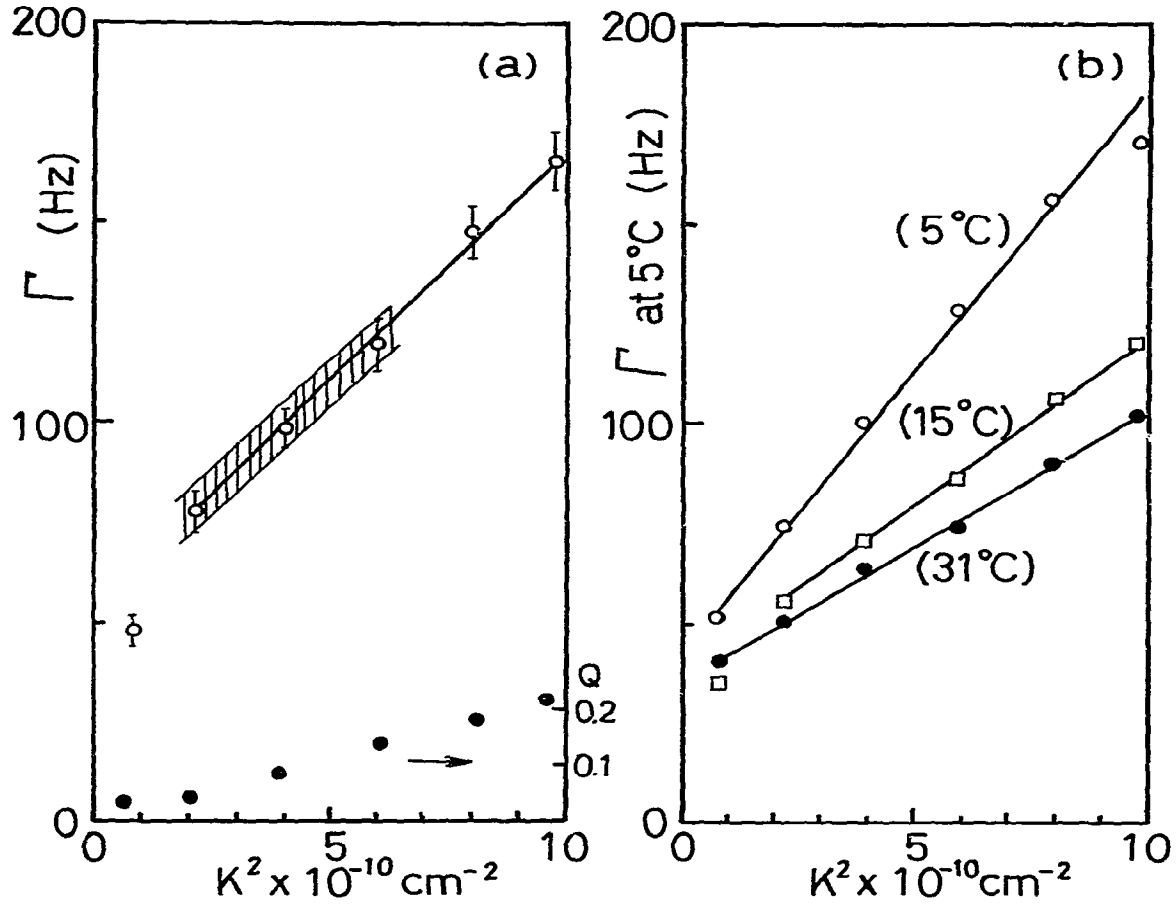

Fig. 12. The Γ vs. K^2 relations of the power spectra for a solution of F-actin at 1 mg/ml. The relations, eqs. 11b, 14b and 17, were used. (a) $T \approx 1$ ms, $N = 1024$, temperature = 15 °C and $\gamma/2\pi \approx 30$ Hz. The shaded area indicates the region where the previous results [1,4,5] are included. The Q vs. K^2 relation is also plotted. (b) Γ vs. K^2 relations at different temperatures after T/η scaling to 5 °C. All the conditions except for temperatures are the same as those in a.

in good agreement with our previous result (the shaded area indicates the region where the previous results are included). In the present approximation of eq. 17, the contribution to $\bar{S}(f)$ from the fast component of fluctuations results in an increase of the Q value (fig. 12a), because very wide Lorentzians with small amplitudes are practically approximated as the frequency-independent component. Note that the K dependence of Q corresponds to the upward deflection of the $\bar{\Gamma}$ vs. K^2 relationship, i.e., $\bar{\Gamma} = A(K^2)K^2$, in the correlation method [6,8]. The quantity Γ is indeed a measure of the spectral width, but it alone has no direct relation with $\bar{\Gamma}$ (see appendix A). [It should be noted that the absolute value of Γ (and also Q) depends on the filter frequency: The choice of

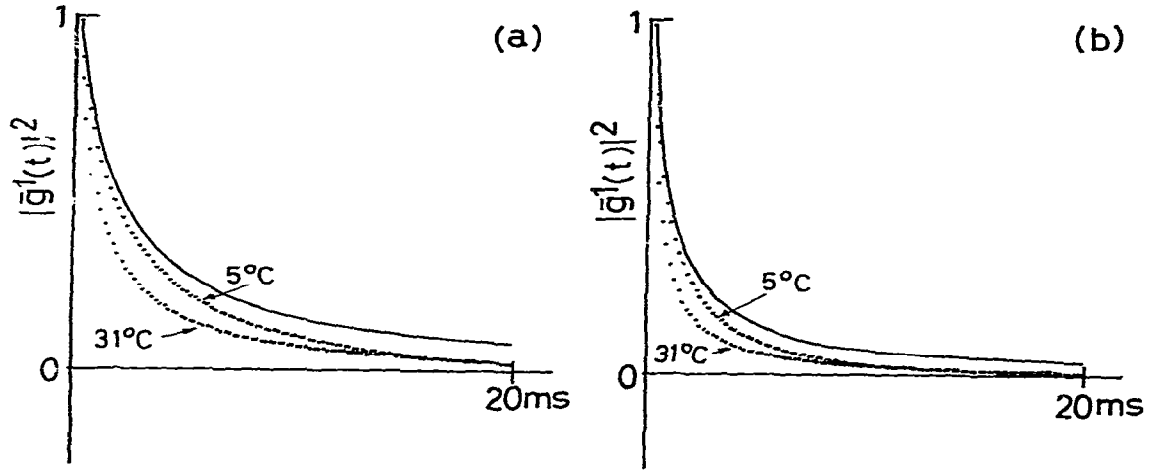

Fig. 13. Correlation functions $[\bar{g}^1(t)]^2$ *of the intensity of light scattered from a solution of F-actin at 1 mg/ml and at 5 and 31 °C.* $T = 0.2$ *ms.* $N = 1024$ *and effective data accumulation period = 80 s × 10 runs. The solid lines represent the correlation functions at 31 °C after* T/η *scaling to 5 °C. The scattering angles are 50 °* (a) *and 90 °* (b). *For* T/η *scaling, see section 4.*

20–30 Hz for $\gamma/2\pi$ reproduced our old results.] In order to see how this Γ vs. K^2 relationship changes with varied environmental conditions, we studied the temperature dependence of power spectra and correlation functions. Fig. 12b shows Γ vs. K^2 relationships at three different temperatures, where Γ values have been corrected with the ratio of the absolute temperature T to the viscosity η. The higher the temperature, the smaller the Γ values corrected to 5 °C. Since it is known that F-actin becomes more flexible as temperature rises, this result indicates that the Γ values decrease when the filament flexibility increases. This is opposite to the change in $\bar{\Gamma}$ of correlation functions, i.e., the initial decay rates $\bar{\Gamma}$ increase as the filament flexibility increases [3]. (For this point, see section 4.) Fig. 13 shows examples of correlation functions $[\bar{g}^1(t)]^2$ at different temperatures. The correlation function at 31 °C decays faster than that at 5 °C, but after T/η scaling the former (the solid line) decays more slowly than the latter at longer time regions. Reflecting this situation, Γ measured at 31 °C and corrected to 5 °C is smaller than Γ measured at 5 °C. The same trend was also observed for F-actin-tropomyosin complexes.

3.1. Some additional results

Fig. 14a shows Γ vs. K^2 relationships at different temperatures for solutions of F-actin at 1 mg/ml. Each point was obtained by a simple average of the results for three preparations, for each of which we made 10 successive measurements. The B values in $\Gamma = AK^2 + B$ are independent of temperature, which confirms our previous experiment [26]. Fig. 14b shows Γ values of 10 successive measurements at each angle for one particular preparation. This gives an idea of the reproducibility of the spectra.

Since each HMM has two active heads (two binding sites to actin), HMM is believed to be a bifunctional cross-linker to F-actin in the absence of ATP. Indeed, the solution of the complex does not pour from an inverted cuvette after hydrolysis of ATP, when 1 mg/ml F-actin and 1 mg/ml HMM are mixed in equal volumes in the presence of ATP. In our previous experiment [4], we also studied the solutions of F-actin complexed with HMM. Since we used the analog method, we could not know the magnitude of β in eq. 15a. Later, Carlson and Fraser [6] reported that the β value

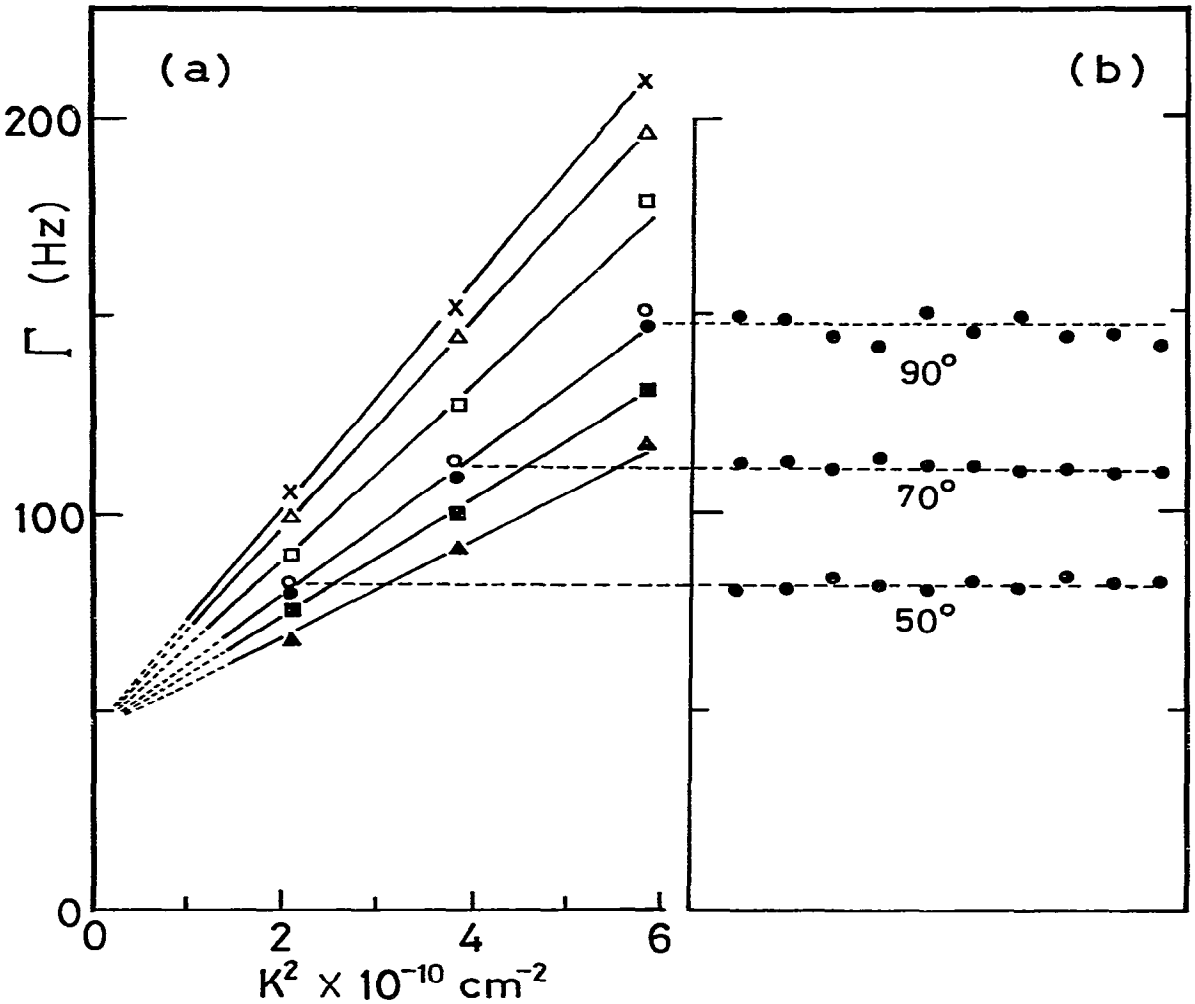

Fig. 14. The Γ vs. K^2 relations of the power spectra for solutions of F-actin at 1 mg/ml. $T = 1$ ms, $N = 1024$ and $\gamma/2\pi = 25$ Hz. (a) Each point was a simple average of the results for three independent preparations, for each of which 10 successive measurements were made. Temperatures: 20 °C (○), 30 °C (□), 40 °C (△), 45 °C (×), 5 °C (▲), 10 °C (■) and 20 °C (●). Note that B in $\Gamma = AK^2 + B$ was independent of temperature. (b) Γ values of 10 successive measurements at each angle for one particular preparation. Temperature: 20 °C.

became almost zero for a solution at 1 mg/ml F-actin and 2 mg/ml HMM after ATP was completely hydrolyzed. Here, we studied this complex again and found that the β value was not small compared with that for F-actin alone. Fig. 15 shows some examples of $\beta[g^1(t)]^2$ for solutions of F-actin-HMM complexes. We have to note that not only the large β value but also fairly good

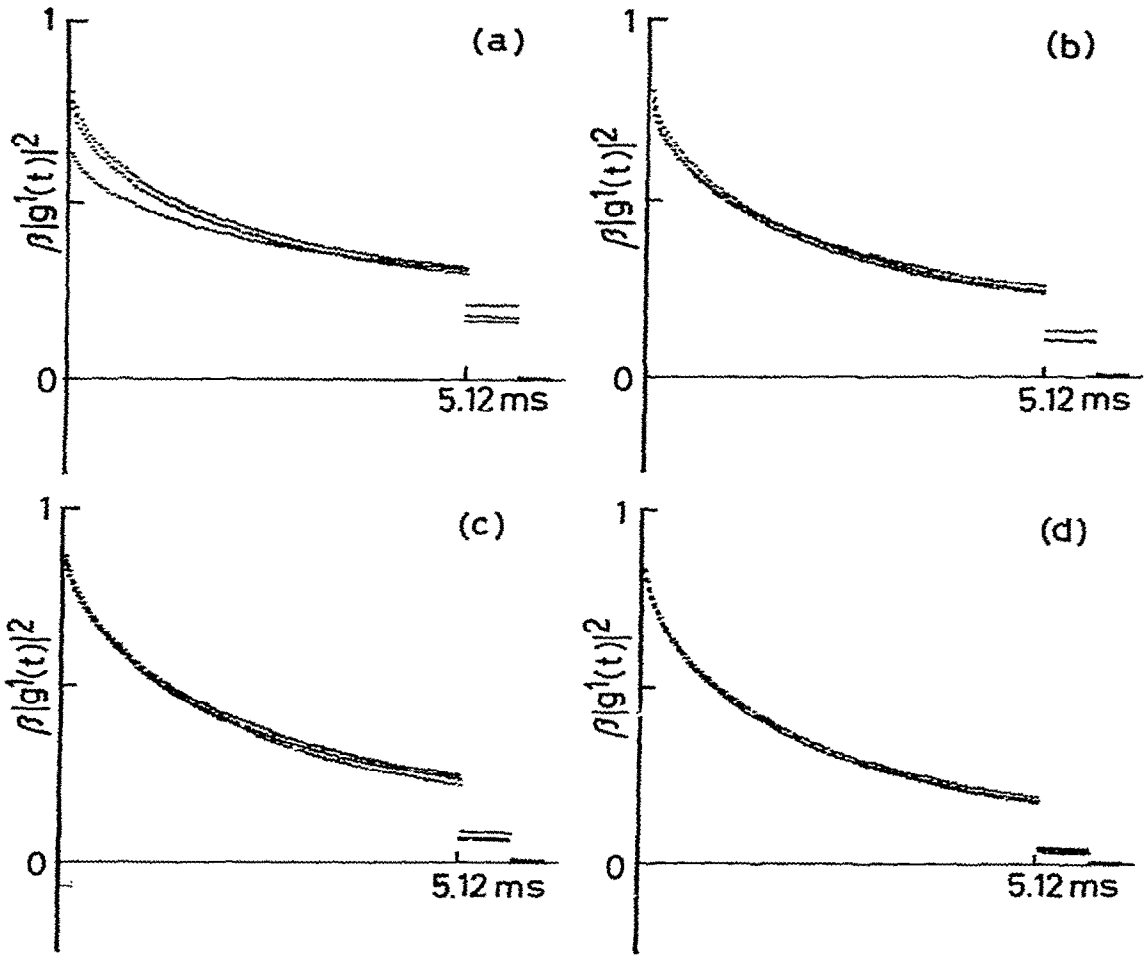

Fig. 15. Some examples of $\beta[g^1(\tau)]^2$ for solutions of F-actin-HMM complexes at 0.5 mg/ml F-actin. Scattering angle, 60°; temperature, 20 °C; and $T = 40$ μs. The weight ratios of F-actin to HMM were 1:1 (a), 1:2 (b), 1:4 (c) and 1:8 (d).

reproducibility of the profiles of correlation functions were observed at this high actin concentration (0.5 mg/ml). Interpretation of this result is not straightforward. A detailed study on F-actin-HMM complexes will be given elsewhere.

4. Discussion

The drastic and large change in the R value in fig. 7 is considered to suggest the transition from a dilute to a semidilute regime. Let c, c_p and c^* be,

respectively, the number of filaments/ml, the filament concentration in units of mg/ml and the critical concentration for filament overlap. It is evident that $cL^3 = c_p/c^*$ where $c^* = M_r/NL^3$ in units of mg/ml (M_r, molecular weight; N, Avogadro's number). Since in vitro reconstituted F-actin has the length distribution given by $N(l) = \langle l \rangle^{-1} \exp(-l/\langle l \rangle)$ with $\langle l \rangle \simeq 0.7$ μm [27], c^* is estimated to be 0.08 mg/ml for $L = \langle l \rangle$ and 0.01 mg/ml for $L = 2\langle l \rangle$. Since the weight average length $L_w = 2\langle l \rangle$ is a representative one in light scattering, the latter value for c^* may be appropriate. From fig. 7, it is inferred that the actual onset of the semidilute region appears to be around 0.3–0.5 mg/ml, which corresponds to $cL^3 = 30$–50 as expected.

Although it is desirable to study the F-actin solution at a dilute regime, very low intensities of scattered light at higher scattering angles make the experiments very difficult. In order to extract the physical properties of F-actin, for example, its flexibility parameter, it seems useful to study correlation functions in the forms of $[g^1_*(t)]^2$ and/or $[\bar{g}^1(t)]^2$ for semidilute solutions. As shown in fig. 7, the decay characteristics of $[g^1_*(t)]^2$ are rather insensitive to the concentration of F-actin. If we had a good theoretical model for computation of correlation functions for semiflexible filaments in semidilute solutions, a comparison between theoretical and experimental $[g^1_*(t)]^2$ and/or $[\bar{g}^1(t)]^2$ would give us information on dynamical properties of individual filaments in the same way as we have discussed for a dilute regime [3,18]. Along this line, we will briefly discuss our model described elsewhere [18].

Let us define the conformation of a long, thin and semiflexible (or slightly bendable) rod by a space curve $\boldsymbol{r}(s, t)$, where s is the coordinate of a segment measured from the center of the rod and t time:

$$\boldsymbol{r}(s, t) = \boldsymbol{R}(t) + s\boldsymbol{t}(t) + \sum_m{}'' \boldsymbol{q}(m, t)Q(m, s) \quad (18)$$

Here, $\boldsymbol{R}(t)$ is the position vector of the center-of-resistance of, and $\boldsymbol{t}(t)$ is the unit vector parallel to the 'mean' axis of, the rod. The term under the summation sign represents the bending motions of the semiflexible rod and the double prime ($''$) denotes exclusion of $m = 0$ and 1. The unnormalized field correlation function $G^1(t)$ of polarized light scattered from a solution of semiflexible filaments in this model is given by

$$G^1(t) = (1/L^2) \int\int_{-L/2}^{L/2} J(s, s', t)\mathrm{d}s\mathrm{d}s' \quad (19)$$

$$J(s, s', t) = \exp(-D_1 K^2 t) \times \langle e^{iK(s\xi - s'\xi')} \prod_m{}'' e^{-\Phi(m, s, s', \xi, \xi', t)} \rangle \quad (20)$$

where L is the contour length of the rod, D_1 the sideways translational diffusion constant and

$$\langle \ldots \rangle = \frac{1}{2} \int\int_{-1}^{1} (\ldots) g_K(\xi, \xi'; t)\mathrm{d}\xi\mathrm{d}\xi' \quad (21)$$

The variable ξ is given by $\cos\theta(t)$, where $\theta(t)$ is the instantaneous angle between vectors $\boldsymbol{K}$ and $\boldsymbol{t}(t)$. With a high accuracy, we can put $\xi = \xi'$ in $\Phi(m, s, s', \xi, \xi', t)$, i.e. [18]

$$\Phi(m, s, s', \xi, \xi, t) = (K^2/4)(1 - \xi^2)\langle q_m^2 \rangle \times \left[Q(m, s)^2 + Q(m, s')^2 - 2Q(m, s)Q(m, s') \times \exp(-t/\tau_m) \right] \quad (22)$$

where $\langle q_m^2 \rangle$ is the expectation value of the square of $\boldsymbol{q}(m, t)$ and τ_m the relaxation time of the mth normal mode of the bending motion. The function $g_K(\xi, \xi'; t)$ is the conditional probability that if the rod is found at orientation ξ' at time zero, it will be found at orientation ξ at time t, and satisfies the diffusion equation:

$$\left[\partial/\partial t - \theta\left(\nabla_\xi^2 - \mu^2 \xi^2 \right) \right] g_K(\xi, \xi'; t) = \delta(\xi - \xi')\delta(t) \quad (23)$$

$$\mu^2 = (D_3 - D_1)K^2/\theta \text{ (the coupling constant)} \quad (24)$$

where θ and D_3 are, respectively, the rotational and the lengthwise translational diffusion constants and $\nabla_\xi^2 = \partial/\partial\xi(1 - \xi^2)\partial/\partial\xi$. The above formulation is valid at $cL^3 \ll 1$ (at dilute regime). At $cL^3 \gg 1$ (at semidilute regime), we follow the

Doi-Edwards model [28]. They assumed

$$\bar{D}_1 = 0,\ \bar{D}_3 = D_3$$
$$\bar{\theta} = \theta/(cL^3)^2 = (D_3/L^2)/(cL^3)^2 \qquad (25)$$
$$\bar{\mu}^2 = (KL)^2(cL^3)^2$$

where bars over various quantities denote those at $cL^3 \gg 1$. Then, $G^1(t)$ at this regime is given by the above equations after simple replacement of D_t values, θ and μ^2 with $\bar{D}_t$ values, $\bar{\theta}$ and $\bar{\mu}^2$, respectively. When $\bar{\mu}^2 \ggg 1$ due to $cL^3 \gg 1$, we have [18]

$$G^1(t) = \operatorname{sech}(\bar{\mu}\bar{\theta}t)\frac{1}{2}\int_{-1}^{1} d\xi \frac{1}{L^2}\int\int_{-L/2}^{L/2} ds\,ds' \times \exp\left[-\frac{K^2(s+s')^2}{4\bar{\mu}}\tanh(\bar{\mu}\bar{\theta}t)\right] \times \exp\left[-\bar{\mu}\xi^2\tanh(\bar{\mu}\bar{\theta}t)\right] e^{iK(s-s')\xi} \times \prod_m{}'' e^{-\Phi(m,s,s',\xi,\xi,t)} \qquad (26)$$

First, we consider the case of rigid rods, i.e., $\langle q_m^2 \rangle = 0$. For short times which satisfy $\tanh(\bar{\mu}\bar{\theta}t) \simeq \bar{\mu}\bar{\theta}t$ and $\operatorname{sech}(\bar{\mu}\bar{\theta}t) \simeq 1$, we have $\bar{\mu}\xi^2\tanh(\bar{\mu}\bar{\theta}t) = D_3K^2t\xi^2$ and $[K^2(s+s')^2/4\bar{\mu}]\tanh(\bar{\mu}\bar{\theta}t) \leq D_3K^2t/[4(cL^3)^2]$, and hence

$$G^1(t) = \int_0^1 [j_0(k\xi)]^2 \exp[-D_3K^2t\xi^2]\,d\xi \qquad (27)$$

where $k = KL/2$ and $j_0(z) = (\sin z)/z$. Eq. 27 includes continuous relaxation rates from 0 to D_3K^2 with weight $[j_0(k\xi)]^2$ which has large values at small ξ for large KL values, and hence $G^1(t)$ has a long tail. For long times which satisfy $\tanh(\bar{\mu}\bar{\theta}t) \simeq 1$ and $\operatorname{sech}(\bar{\mu}\bar{\theta}t) = \exp(-\bar{\mu}\bar{\theta}t)/2$, eq. 26 gives $G^1(\tau) \propto \exp[-D_3K^2t/(KL \times cL^3)]$. Thus, the long tail of $G^1(t)$ decays indeed very slowly.

Now, we consider semiflexible filaments in a semidilute solution. For a short time $t = 3\tau_2 \lll 1/(\bar{\mu}\bar{\theta})$, we have $\Phi(m, s, s', \xi, \xi, 3\tau_2) \simeq \Phi(m, s, s', \xi, \xi, \infty)$. Thus, for $t \gtrsim 3\tau_2$, the time dependence of eq. 26, which we denote as $G_{tr}(t)$, is the same as that for a rigid rod in a semidilute solution, i.e., $G_{tr}(t)$ has a long tail as in the case of $G^1(t)$ in eq. 27. Within a very short time, $G^1(t)$ in eq. 26 decays from $G^1(0)$ to $G^1(3\tau_2)$ $[\equiv G_{tr}(3\tau_2)]$. The amplitude of the initial fast decay due to bending motions, $[G^1(0) - G_{tr}(3\tau_2)]/G^1(0)$, depends on both γL and KL values. Now, when we write

$$|G^1(t)|^2 \equiv |G_{tr}(t)|^2 + \left[|G^1(t)|^2 - |G_{tr}(t)|^2\right] \qquad (28)$$

the second term on the right-hand-side of eq. 28 mostly results from contributions of bending motions, and the first term $|G_{tr}(t)|^2$ will be eliminated in the expressions of $[g_*^1(t)]^2$ and $[\bar{g}^1(t)]^2$. This situation is compatible with the experimental findings, at least qualitatively.

Simulated correlation functions based on eq. 26 agree qualitatively with our experimental results [30,31]. However, a quantitative agreement has not been obtained. These difficulties probably arise from the following facts. The original Doi-Edwards model assumes (eq. 25) $\bar{\theta} = k_1\theta/(cL^3)^2$, where k_1 is a proportionality constant (expected to be within an order of 10). Since $cL^3 = c_p/c^*$, we have $\theta/\bar{\theta} = (1/k_1)(c_p/c^*)^2$. From experimental data for rod-like viruses obtained from transient electric birefringence measurements [32], we can estimate the k_1 value to be about 5000 for M-13-WT ($L = 0.892$ μm, $d = 8.5$ nm and $M_r = 1.6 \times 10^7$) and about 17000 for M-13-T_n3-15 ($L = 1.58$ μm, $d = 8.5$ nm and $M_r = 2.28 \times 10^7$). Both values are very much larger than expected. The same situation has also been reported for other cases. From depolarized light scattering measurements [33], it is reported that the k_1 values for PBLG with $M_r = 150000$, 170000 and 210000 are 1070, 1170 and 1786, respectively. From dynamic electric birefringence measurements [34], the low relaxation frequency $\bar{f}_L$ was found to be 77 Hz for 1 wt.% PBLG with $M_r = 150000$. The Doi-Edwards model gives $\bar{f}_L = 0.11$ Hz, resulting again in a difference of 700-fold. Although almost complete c^{-2} and fairly good L^{-9} dependences are confirmed in any case cited above, the absolute value of $\bar{\theta}$ is several orders of magnitude larger than predicted. Another problem is specific to polarized light scattering. For a very long filament, $L = 1$ μm and $cL^3 = 64$, for example, correspond to four filaments per μm or 250 nm per filament. This means that a filament is confined in a cage with a diameter of about 250 nm. The sideways translation of the filament in the cage could be detected,

because we have $1/K = 100$ nm even for such a low angle as $K^2 = 1 \times 10^{10}$ cm^{-2}. That is, even if $\bar{D}_1 = k_2 D_1/(cL^3)^2$ is assumed instead of $\bar{D}_1 = 0$ in the original Doi-Edwards model (eq. 25), the proportionality constant k_2 would have a very large value as does k_1. Our alternatives, $\bar{\theta} = k_1'\theta/(cL^3)$ and $\bar{D}_1 = k_2' D_1/(cL^3)$ [35], still entail problems; both k_1' and k_2' will be much larger than 10. Unexpected light scattering results for M-13-WT [26] might result from these reasons. A trial to analyze these data has been made, which suggested $\bar{D}_1 = 0.5 D_1$ at $K^2 = 1.5 \times 10^{10}$ cm^{-2} and $\bar{D}_1 = D_1$ at $K^2 = 4 \times 10^{10}$ cm^{-2} [18].

When the correlation functions $[g^1(t)]^2$ at temperatures T_h and T_l ($T_h > T_l$) can scale with T/η, the spectral with $\Gamma_{s,h}$ and $\Gamma_{s,l}$ of $S(f)$ (see appendix A for definition of Γ_s) will also scale with T/η. For T/η scaling of Γ from $\bar{S}(f)$, on the other hand, we have to take account of the choice of filter frequency. In the above situation, we will have a scaling relationship $(T_l/\eta_l)\Gamma_h = (T_h/\eta_h)\Gamma_l$, provided that Γ_h and Γ_l are determined from $\bar{S}(f)$ values at the filter frequencies γ_h and γ_l, respectively, which satisfy $(T_l/\eta_l)\gamma_h = (T_h/\eta_h)\gamma_l$. The Γ values for F-actin scaled in this sense are shown in fig. 16, where (○) shows Γ_l at $T_l = 5\,^\circ$C and $\gamma_l/2\pi = 30$ Hz, (■) Γ_h/α at $T_h = 31\,^\circ$C and $\gamma_h/2\pi = \alpha\gamma_l/2\pi = 60$ Hz (note that $\alpha \equiv (T_h/\eta_h)/(T_l/\eta_l) = 2.13$), (□) Γ_h/α at $T_h = 31\,^\circ$C and $\gamma_h/2\pi = 30$ Hz and (●) Γ_l at $T_l = 5\,^\circ$C and $\gamma_l/2\pi = (1/\alpha)\gamma_h/2\pi = 15$ Hz. In both cases, (○, ■) and (●, □), Γ values at the lowest K^2 values coincide with each other as expected, whereas Γ values at larger K^2 values do not scale with T/η. Because D_t values and θ (and hence $\bar{D}_t$ values and $\bar{\theta}$) are proportional to T/η, $G^1(t)$ in eq. 26 can scale with T/η, provided that the flexibility parameter (γL) is independent of temperature (note that for a given length L, $\langle q_m^2 \rangle$ depends only on the (γL) value and $\tau_m^{-1} \propto (T/\eta)/\langle q_m^2 \rangle$ [29]). The nonscaling property of Γ shown in fig. 16 probably means that $\gamma L (\neq 0)$ depends on temperature. This is compatible with the experimental results by other techniques [13–17]. They showed that the actin filament becomes more flexible (the γL value becomes larger) when the temperature is raised. The reason is not simple, however, why Γ_h/α is smaller than Γ_l in fig. 16. This probably results mainly

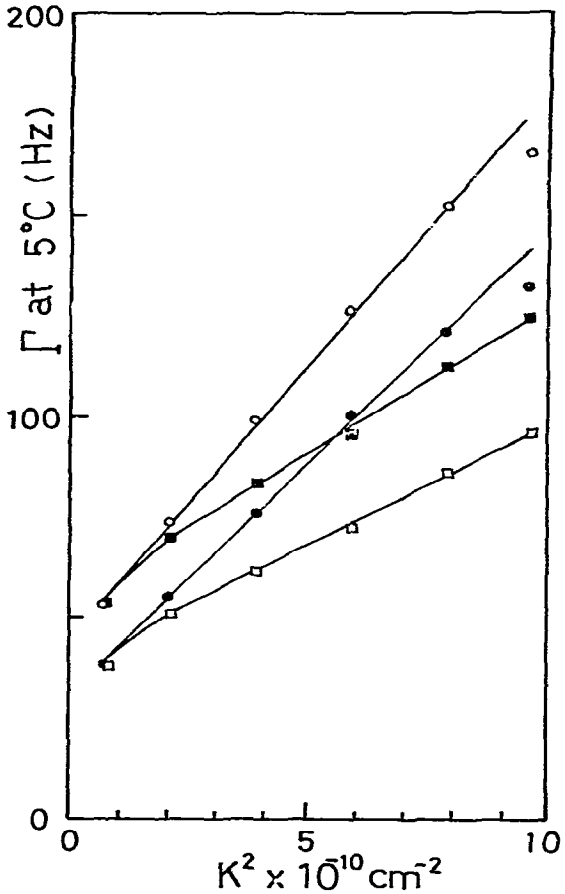

Fig. 16. The Γ vs. K^2 relations after T/η correction to 5 °C. F-Actin at 1 mg/ml, $T = 1$ ms and $N = 1024$. (○) Γ_l at $T_l = 5\,^\circ$C and $\gamma_l/2\pi = 30$ Hz, (■) Γ_h/α at $T_h = 31\,^\circ$C and $\gamma_h/2\pi = \alpha\gamma_l/2\pi = 60$ Hz, (□) Γ_h/α at $T_h = 31\,^\circ$C and $\gamma_h/2\pi = 30$ Hz, and (●) Γ_l at $T_l = 5\,^\circ$C and $\gamma_l/2\pi = (1/\alpha)\gamma_h/2\pi = 15$ Hz. Note that $\alpha \equiv (T_h/\eta_h)(T_l/\eta_l) = 2.13$ (for details, see text).

from the fitting procedure by use of eq. 17, because more involvement of the internal flexing modes causes an increase in the amplitude of the far wings of $\bar{S}(f)$ which results in a larger Q value. The width Γ of $\bar{S}(f)$ is inferred to be mainly determined from the shape of a tail portion in the

initial fast-decaying component of $|G^1(t)|^2$ or $|G^1(t)|^2 - |G_{tr}(t)|^2$ in eq. 28. At any rate, the results in fig. 16 suggest an empirical rule that the more flexible the filament, the smaller the Γ value at least for F-actin in semidilute solutions. This agrees with our previous conclusions [4,5].

5. Conclusions

The profiles of successively measured intensity autocorrelation functions of polarized light scattered from solutions of in vitro reconstituted F-actin were highly reproducible below 0.2 mg/ml actin and highly nonreproducible above 0.3 mg/ml actin. This behavior could be interpreted as a transition from a dilute to a semidilute regime. Even at 1 mg/ml F-actin ($cL^3 \simeq 100$ if $L_w \simeq 1.4$ μm was assumed), on the other hand, profiles of $[g^1_*(t)]^2$ and $[\bar{g}^1(t)]^2$ showed a fairly good reproducibility, suggesting that nonreproducibility of the profiles of $[g^1(t)]^2$ arises from the existence of a very slow mode. The fact that $cL^3 = 100$ is close to $L/d \simeq 180$ (if $d = 8$ nm is assumed for the diameter of F-actin), suggests an occurrence of aggregates of filaments (liquid crystalline particles). Several pieces of evidence, however, excluded the possibility that an occupation number fluctuation in the scattering volume of these aggregated particles could account for the above-mentioned slow mode. The slow mode indeed resulted from such slow fluctuations that the data accumulation period of 3600 s/run was not long enough to obtain a high statistical accuracy. We inferred that the slow mode arose from the restricted translational/rotational Brownian motion of the filament. The initial fast decay of $[g^1(t)]^2$ was concluded to result mostly from bending motions of the filament, because $[g^1_*(t)]^2$ (and also $[\bar{g}^1(t)]^2$) showed little concentration dependence from 0.01 to 1 mg/ml F-actin. A theoretical model was discussed, which could explain the initial fast decay followed by a very slow one of $[g^1(t)]^2$. The model agreed with the present experimental results qualitatively but not quantitatively. Difficulties might arise from the poor knowledge at present about k_1 and k_2 in $\bar{\theta} = k_1\theta/(cL^3)^2$ and $\bar{D}_1 = k_2 D_1/(cL^3)^2$, respectively.

An analysis of power spectra $\bar{S}(f)$ obtained by the fast Fourier method confirmed our previous experimental results. Since $\bar{S}(f)$ lacked information about frequency components lower than $1/2NT$ Hz (or $\gamma/2\pi$ Hz), its profiles even for a 1 mg/ml solution were highly reproducible just as those of $[g^1_*(t)]^2$ and $[\bar{g}^1(t)]^2$ were. A comparison of power spectra $\bar{S}(f)$ and correlation functions $[\bar{g}^1(t)]^2$ computed from the same data of $\{n(t + mT, T)\}$ on magnetic tapes clarified the reasons why the bandwidth Γ of $\bar{S}(f)$ [1,4,5] largely differed from the bandwidth Γ of $[g^1(t)]^2$ [6–8]. The most important reason was that our previous a.c.-coupled spectral method did not detect the very slow component, which would convey little or no information of the filament flexibility but affect the correlation function very strongly. Even after very slow components were eliminated, the Γ values were much smaller than the $\bar{\Gamma}$ values of $[\bar{g}^1(t)]^2$. This is a natural consequence of the fact that an analysis in the frequency domain picks more information up from low-frequency components whereas an analysis in the time domain picks more information up from fast components. The temperature dependence of Γ suggested that F-actin would have some flexibility and that the flexibility parameter would change with temperature.

Although some progress has been made, we are still far from a perfect situation for the analysis of spectral data (both power spectra and correlation functions) of F-actin solutions at dilute and semidilute regimes. More experimental and theoretical studies will be required not only for F-actin but also for other types of long filaments such as long viruses [36]. We will discuss elsewhere further studies including the case of F-actin-HMM complexes briefly mentioned in section 3.

Appendix A. A comment on Γ and $\bar{\Gamma}$

Let us consider a wide distribution of decay rates $P(\Gamma)$. The field correlation function and the corresponding homodyne power spectrum are given, respectively, by

$$g^1(t) = \sum_n P(\Gamma_n) \exp(-\Gamma_n t) \quad \text{with} \quad \sum_n P(\Gamma_n) = 1 \tag{A1}$$

$$S(\omega)=\frac{1}{\pi}\int_0^\infty [g^1(t)]^2\cos(\omega t)\mathrm{d}t$$
$$=\frac{1}{\pi}\sum_n\sum_m P(\Gamma_n)P(\Gamma_m)\frac{(\Gamma_n+\Gamma_m)}{\omega^2+(\Gamma_n+\Gamma_m)^2} \quad (A2)$$

The initial decay rate $\bar{\Gamma}$ of $g^1(t)$ is given by

$$\bar{\Gamma}=-\lim_{t\to 0}\frac{\mathrm{d}}{\mathrm{d}t}g^1(t)=\sum_n P(\Gamma_n)\Gamma_n \quad (A3)$$

For a high frequency ω_h which satisfies $\omega_h^2 \gg (\Gamma_n+\Gamma_m)^2$ for any pair of n and m, we have from eq. A2

$$S(\omega_h)=\frac{1}{\pi}\sum_n\sum_m P(\Gamma_n)P(\Gamma_m)(\Gamma_n+\Gamma_m)/\omega_h^2$$
$$=(2/\pi)\bar{\Gamma}/\omega_h^2 \quad (A4)$$

Thus, we have $\bar{\Gamma}=(\pi/2)\omega_h^2 S(\omega_h)$ [3], which is rather related to Q in our analysis. The spectral width Γ_s will be defined by

$$\Gamma_s^{-1}=\lim_{\omega\to 0}2\pi S(\omega)=2\sum_n\sum_m P(\Gamma_n)P(\Gamma_m)/$$
$$(\Gamma_n+\Gamma_m)=2\int_0^\infty [g^1(t)]^2\mathrm{d}t \quad (A5)$$

Thus, we have $\bar{\Gamma}\geq\Gamma_s$, where $\bar{\Gamma}=\Gamma_s$ only for $P(\Gamma_n)=\delta(\Gamma_n-\bar{\Gamma})$. Eq. A5 cannot be applied to $\bar{S}(\omega)$ because of $\bar{S}(0)=0$. Roughly speaking, however, Γ of $\bar{S}(\omega)$ will approximately be given by

$$\Gamma^{-1}=2\sum_n{}'\sum_m{}' P(\Gamma_n)P(\Gamma_m)/(\Gamma_n+\Gamma_m) \quad (A6)$$

where primes denote the exclusion of terms for which $(\Gamma_n+\Gamma_m)\leq\gamma$ is satisfied. Although Γ is a measure of the spectral width, it has no direct relation with $\bar{\Gamma}$.

References

1 S. Fujime, J. Phys. Soc. Jap. 29 (1970) 751.
2 S. Fujime and M. Maruyama, Macromolecules 6 (1973) 237.
3 T. Maeda and S. Fujime, Macromolecules 14 (1981) 809.
4 S. Fujime and S. Ishiwata, J. Mol. Biol. 62 (1971) 251.
5 S. Ishiwata and S. Fujime, J. Mol. Biol. 68 (1972) 511.
6 F.D. Carlson and A.B. Fraser, J. Mol. Biol. 89 (1974) 237.
7 A.B. Fraser, E. Eisenberg, W.W. Kielley and F.D. Carlson, Biochemistry 14 (1975) 2207.
8 T. Maeda and S. Fujime, J. Phys. Soc. Jap. 42 (1977) 1983.
9 A. Hochberg, W. Low, R. Tirosh, J. Borejdo and A. Oplatka, Biochim. Biophys. Acta 460 (1977) 308.
10 J. Newman and F.D. Carlson, Biophys. J. 29 (1980) 37.
11 Y. Umazume and S. Fujime, Biophys. J. 15 (1975) 163.
12 S. Yoshino, Y. Umazume, R. Natori, S. Fujime and S. Chiba, Biophys. Chem. 8 (1978) 317.
13 T. Takebayashi, Y. Morita and F. Oosawa, Biochim. Biophys. Acta 492 (1977) 357.
14 H. Nagashima and S. Asakura, J. Mol. Biol. 136 (1980) 169.
15 T. Yanagida and F. Oosawa, J. Mol. Biol. 126 (1978) 501.
16 T. Yanagida and F. Oosawa, J. Mol. Biol. 140 (1980) 313.
17 S. Yoshino and S. Fujime, in: Muscle contraction: its regulatory mechanisms, eds. S. Ebashi, K. Maruyama and M. Endo (Japan Science Society Press, Tokyo/Springer Verlag, Berlin, 1980) p. 181.
18 T. Maeda and S. Fujime, Macromolecules (1984) in the press.
19 S.O. Rice (1944). See C. Kittel, Elementary statistical physics (John Wiley, New York, 1958) p. 117.
20 S.-H. Chen, W.B. Veldkamp and C.C. Rai, Rev. Sci. Instrum. 46 (1975) 1356.
21 F.B. Straub, Stud. Inst. Med. Chem. Univ. Szeged 3 (1943) 23.
22 J.A. Spudich and S.J. Watt, J. Biol. Chem. 246 (1971) 4866.
23 S. Ebashi, A. Kodama and F. Ebashi, J. Biochem. (Tokyo) 64 (1968) 465.
24 A.G. Weeds and B. Pope, J. Mol. Biol. 111 (1977) 129.
25 A. Szent-Györgyi, Chemistry of muscle contraction, 2nd edn. (Academic Press, London, 1951).
26 S. Ishiwata, Ph.D. thesis, Nagoya University (1975).
27 M. Kawamura and K. Maruyama, J. Biochem. (Tokyo) 66 (1970) 619.
28 M. Doi and S.F. Edwards, J. Chem. Soc. Faraday II 74 (1978) 560.
29 S. Fujime and T. Maeda, Biophys. J. 38 (1982) 213.
30 S. Fujime, T. Maeda and S. Ishiwata, in: Biomedical applications of laser light scattering, eds. D.B. Sattelle, W.I. Lee and B.R. Ware (Elsevier, Amsterdam, 1982) p. 251.
31 S. Fujime, S. Ishiwata and T. Maeda, in: The applications of laser light scattering to the study of biological motion, eds. J.C. Earnshaw and M.W. Steer (Plenum Press, New York, 1983) p. 459.
32 J.F. Maguire, J.P. McTague and F. Rondelez, Phys. Rev. Lett. 45 (1980) 1891; J.F. Maguire, J.P. McTague and F. Rondelez, Phys. Rev. Lett. 47 (1981) 148.
33 K.M. Zero and R. Pecora, Macromolecules 15 (1982) 87.
34 Y. Mori, N. Ookubo, R. Hayakawa and Y. Wada, J. Polym. Sci. Phys. 20 (1982) 2111.
35 T. Maeda and S. Fujime (1984) Macromolecules, in the press.
36 J.F. Maguire, J. Chem. Soc. Faraday II 77 (1981) 513.